ACS APPLIED NANO MATERIALS

www.acsanm.org Article

Digestive Ripening-Mediated Growth of $NaYbF_4$:Tm@$NaYF_4$ Core–Shell Nanoparticles for Bioimaging

Chunyu Qi, Li Chen,* Yuan Gao, Yue Wang, Jing Li, Ligong Zhang, Yongshi Luo, and Xiaojun Wang

Cite This: *ACS Appl. Nano Mater.* 2020, 3, 10049–10056 Read Online

ACCESS | Metrics & More | Article Recommendations | Supporting Information

ABSTRACT: Size and size distribution control along with the excitation/emission wavelength manipulation are the most indispensable for both fundamental research and applications of upconverting nanophosphors. In contradiction to the usual Ostwald ripening process, digestive ripening-mediated growth of core–shell nanostructures is observed in a lanthanide-doped ternary fluoride system. Time-dependent size evolution of $NaYbF_4$:Tm@$NaYF_4$ nanoparticles is systematically investigated, and a K_{sp}-involved growth mechanism is proposed to better understand this unusual phenomenon. The upconversion luminescence (UCL) intensity and branch ratio of near-infrared to visible emission (NIR/VIS) dramatically increase due to the $NaYF_4$ coating but subsequently undergo a decline when an additional SiO_2 layer grows outside. As a comparison, an alternant type of core–shell–shell nanostructure, $NaYbF_4$:Tm@SiO_2@$NaYF_4$, is further constructed, in which both the UCL intensity and NIR/VIS ratio exhibit an inverse trend. The comparative analysis on the basis of steady and transient spectroscopic data from $NaYbF_4$:Tm, and alternatively coated by silica and $NaYF_4$ nanoshells, respectively, demonstrates that the UCL properties can be regulated through core–shell engineering once the optical behavior of the surface states can be manipulated. The results provide a promising alternative strategy to fabricate a uniform core–shell nanostructure with multicompositions, and this NIR_{in}–NIR_{out} luminescent profile deserves an expectable vision for the subsequent clinical applications of UCL imaging for deep biological tissues.

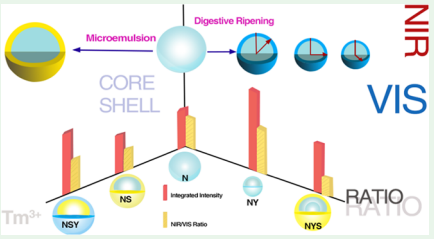

KEYWORDS: *digestive ripening, core–shell nanostructure, upconversion luminescence, Ostwald ripening, alternatively coating, lanthanide-doped fluorides*

Downloaded via JILIN UNIV on April 11, 2021 at 11:42:39 (UTC).
See https://pubs.acs.org/sharingguidelines for options on how to legitimately share published articles.

INTRODUCTION

Upconverting lanthanide-doped nanophosphors has a great perspective in both fundamental research[1,2] and a wide range of applications such as high-resolution biological imaging, temperature sensing, photothermal therapy, anticounterfeiting, drug delivery, and photovoltaics.[3−9] Compared with semiconductor quantum dots and organic fluorophores, these upconversion nanoparticles (UCNPs) have unique optical characteristics of sharp emission bandwidth and high photochemical stability, especially the competitively inherent penetration depth advantage of the excitation/emission regions.[10] Therefore, the lanthanide-doped photon upconversion process has attracted more and more attention in biomedicine and information technology.[11] Regarding fundamental research and application domains, control of their size and homogeneous distribution is indispensable thereafter to ascribe the physical properties to each particle. Until now, many preparation protocols have been developed, including microemulsion, hydrothermal/solvothermal, coprecipitation, microwave-assisted, or pyrolysis methods, to synthesize UCNPs with different sizes and morphologies.[12−16] Shi et al. synthesized about 7 nm hexagonal $NaYbF_4$ nanocrystals by a one-pot reaction without doping additional impurities.[17] The crystalline growth mechanism during most of these synthesis processes follows the principle of Ostwald ripening (OR), which refers to that the smaller crystals or particles dissolve and redeposit on the larger ones.[18] In the early 21st century, an inverse OR, named digestive ripening (DR) process, has been reported mostly for the synthesis of pure metal nanoparticles and whereafter for the binary but very rarely for the ternary composition system.[19] DR process features are that the larger particles become smaller and the size distribution turns to be narrower during synthesis.

There are a few papers that have presented insights underlining this novel phenomenon in consideration of the reaction time as well as the temperature.[20] However, a complete understanding of the real nature of this unusual process is still needed to be further developed, especially in a complex composition system.

Because the surface effects play an almost decisive role in impacting the efficiency of UCL, surface engineering such as building a core–shell structure has been conducted to improve the quantum yield, which is the main setback for upconverting

Received: July 29, 2020
Accepted: September 25, 2020
Published: September 25, 2020

© 2020 American Chemical Society

https://dx.doi.org/10.1021/acsanm.0c02057
ACS Appl. Nano Mater. 2020, 3, 10049–10056

nanophosphors to be widely applied. Although considerable progress has been made in the past decades, intensive studies on energy migration on the surface of upconversion nanoparticles are insufficient so far.[21] To improve the UCL efficiency of lanthanum-doped nanocrystals, some strategies have been utilized, such as host lattice manipulation,[22] energy transfer modulation,[23] broadband sensitization,[24] surface plasma coupling,[25] and inert shell coating.[26] Among these methods, core−shell engineering is one of the effective ways to improve the luminescence efficiency.[27] A common method of controlling UCL color is to change the doped ions within the nanoshell. For example, Marta et al. demonstrated that the position of the dopant in the nanoparticles affects luminescence. They synthesized nanoparticles with $NaGdF_4$:Tm^{3+},Yb^{3+} and $NaGdF_4$:Er^{3+},Yb^{3+} by a microwave-based pyrolysis process. The formation of core−shell and core−shell−shell nanoarchitectures using this technique allows doping with both pairs of dopants, spatially separated in the nanoparticles. The color of the entire emission has been adjusted based on tuning the intensity ratio of different emission bands by means of changing the position of the dopant inside the nanostructures.[28] Although the core−shell nanostructure can be used to realize finely regulated Gd-based upconversion nanoparticles with multicolors,[29] simultaneously tuning the intensity and color by means of alternatively coating different types of nanoshells has never been investigated in detail so far.

In the current contribution, the time-dependent size evolution of $NaYbF_4$:Tm@$NaYF_4$ core−shell nanoparticles following a DR process has been investigated in detail at a certain temperature. A K_{sp}-involved recrystallization mechanism is put forward to understand the shrinking of particle size in our synthesis condition. In addition, $NaYbF_4$:Tm@SiO_2@$NaYF_4$ and $NaYbF_4$:Tm@$NaYF_4$@SiO_2 nanostructures were deliberately fabricated. Interestingly, both the UCL intensity and the NIR/VIS ratio of core−shell−shell nanoparticles are alternatively modulated by such a facile core−shell strategy. A reasonable insight into the quenching/enhancement mechanism of integrated intensity and NIR/VIS ratio is discussed based on the analysis of the electronic spectroscopy data and the microstructure characterization. The results offer a promising alternative method to achieve fluoride upconverting nanophosphors with narrower size distribution and simultaneously controllable UCL intensity and color. At the same time, lanthanide-based upconversion nanoparticles can convert low-energy photons into high-energy radiation; nanocomposites with homogeneous morphology and NIR-in-NIR-out emission profile, plus their low biological toxicity, are very promising nanosized multifunctional reagents to be used in *in vivo* deep luminescent diagnostic or even real clinical therapy of diseases in the near future.[30−32]

EXPERIMENTAL SECTION

Materials and Characterizations. Ytterbium (III) acetate hydrate ($Yb(Ac)_3$, 99.9%) and thulium (III) acetate hydrate ($Tm(Ac)_3$, 99.9%) were purchased from Sigma-Aldrich. Oleic acid (OA, 90%), 1-octadecene (ODE, 90%), NH_4F (≥98%, ACS reagent), NaOH, tetraethyl orthosilicate (TEOS, 99% analytical reagent A.R.), ammonia solution, and CO-520 were obtained from Aladdin. $YCl_3·6H_2O$ and $YbCl_3·6H_2O$ were prepared by dissolving the corresponding oxides in diluted hydrochloric acid. Deionized water was used for the preparation of the solutions. All chemicals were used as received without further purification.

Powder X-ray diffraction (XRD) data was collected using Cu Kα radiation (λ = 1.54056 Å) on an X-ray powder diffractometer (Rigaku D/Max IIA). Transmission electron microscopy (TEM) images were obtained by a transmission electron microscope (JEM-2000EX) operating at an acceleration voltage of 200 kV. The UCL spectra were recorded with a spectrophotometer (Edinburgh FSL-920), and infrared spectra were obtained using a Triax 550 spectrometer (Jobin-Yvon) pumped with a power-controllable 980 nm diode laser at room temperature. In fluorescence lifetime measurements, an optical parametric oscillator (OPO) was tuned to 980 nm as an excitation source, and the signals were detected by a Tektronix Digital Oscilloscope (TDS 3052). Infrared spectra in transmission mode were obtained on a Thermo Fisher Nicolet IS50 Fourier transform infrared (FT-IR) spectrometer. The high-resolution transmission electron microscopy (HR-TEM) images were taken on an FEI high-resolution transmission electron microscope.

Synthesis of $NaYbF_4$:Tm Nanoparticles. Tm-doped $NaYbF_4$ nanoparticles were prepared according to the literature procedure.[16,33] Typically, in a 50 mL round-bottom flask, a mixture of Ln_2O_3 and $Ln(Ac)_3$ (0.835 mmol, Ln = Yb^{3+},Tm^{3+}), oleic acid (6 mL), and 1-octadecene (15 mL) was heated at 150 °C for 1 h to form the lanthanide−oleate precursor. After cooling down to room temperature, a methanol solution of NaOH and NH_4F (2 mL) was added to the solution. The resulting mixture was heated at 70 °C for 30 min, then to 300 °C, kept for 1.5 h, and cooled down to room temperature. The resulting nanocrystals were precipitated by the addition of ethanol, collected by centrifugation, and washed with ethanol. The obtained products were then dispersed in cyclohexane and centrifuged to remove the NaF byproducts. Finally, the as-synthesized $NaYbF_4$:Tm nanocrystals were redispersed in cyclohexane (7 mL) for further use. The heating reactions were all conducted in a nitrogen atmosphere.

Synthesis of $NaYbF_4$@$NaYF_4$ Nanocrystals. The core−shell nanoparticles were synthesized by the obtained $NaYbF_4$ nanocrystals as seeds. In a typical experiment, a mixture of YCl_3 (0.2 mmol), oleic acid (6 mL), and 1-octadecene (15 mL), in a 50 mL round-bottom flask, was stirred at 150 °C for 1 h. After cooling down to room temperature, $NaYbF_4$ core nanocrystals, ∼100 nm in cyclohexane, were added to the flask, followed by heating at 80 °C to remove cyclohexane. Thereafter, a methanol solution of NaOH (1 mL, 0.5 M) and NH_4F (2 mL, 0.4 M) was added at room temperature. The resulting mixture then was stirred at 100 °C for 30 min to remove the methanol and heated at 320 °C for 1.5 h. The products were precipitated out with ethanol and collected with centrifugation after the reaction mixture cooled down to room temperature. Finally, the resulting nanocrystals were washed with ethanol and redispersed in cyclohexane (7 mL) for further use. The heating reactions were all conducted in the nitrogen atmosphere.

Synthesis of $NaYbF_4$@SiO_2 Nanocrystals. The core−shell nanoparticles were synthesized by a microemulsion method according to a literature procedure.[35,36] In a typical reaction, we took the prepared $NaYbF_4$ (9 mL), cyclohexane (8 mL), and CO-520 (1 mL) and put them in a small beaker; the resulting mixed solution was dispersed for 1 min by an ultrasonic disperser. Then, ammonia (100 μL) was added to the solution and the solution was stirred for 20 min. After that, TEOS (50 μL) was added to the solution and the solution was stirred at about 600 rpm for 4 h. The resulting products were collected by centrifugation; then, the resulting nanocrystals were washed three times with ethanol and redispersed in water for further use. The thickness of the SiO_2 shell can be controlled by the ratio of CO-520 to TEOS.

Synthesis of $NaYbF_4$@$NaYF_4$@SiO_2 Nanocrystals. The synthesis procedure for $NaYbF_4$@$NaYF_4$@SiO_2 nanoparticles was identical to that for $NaYbF_4$@SiO_2 nanoparticles except for the use of a core stock solution of $NaYbF_4$@$NaYF_4$.

Synthesis of $NaYbF_4$@SiO_2@$NaYF_4$ Nanocrystals. The synthesis procedure for $NaYbF_4$@SiO_2@$NaYF_4$ nanoparticles was a hydrothermal method. In a typical experiment, a mixture of NaOH (1 mL, 0.5 M), NH_4F (2 mL, 0.4 M), oleic acid (5 mL), H_2O (1.5 mL), and ethanol (10 mL), in a 50 mL beaker, was stirred at about 800 rpm

https://dx.doi.org/10.1021/acsanm.0c02057
ACS Appl. Nano Mater. 2020, 3, 10049−10056

for 30 min. Then, $Y(Cl)_3$ (0.2 mmol) was added and kept stirring. Next, the H_2O solution of $NaYbF_4@SiO_2$ was added to the solution and kept stirring for 30 min. Then, the stirred solution was transferred to the reactor and heated at 200 °C for 8 h. The products were precipitated out with ethanol and collected with centrifugation after the reaction mixture cooled down to room temperature. Finally, the resulting nanocrystals were washed with ethanol and redispersed in cyclohexane (7 mL) for further use.

RESULTS AND DISCUSSION

Crystalline Growth of Upconverting Nanophosphors.

A series of samples have been designed and fabricated through a modified pyrolysis protocol, including $NaYbF_4$:Tm nanoparticles (designated as N) as a luminescent core, coated with different types of shells in a few nanometers of thickness on the surface. In the case of silica coating, the core size nearly retains its initial dimension and becomes a little larger after being covered by a thin layer of SiO_2. However, in synthesizing $NaYbF_4$:Tm@$NaYF_4$ (NY) nanoparticles for comparison, the core size is surprisingly found to be smaller as the reaction time increases and consequently the $NaYF_4$ nanoshell forms outside the $NaYbF_4$:Tm nanocrystal. These crystalline growth processes are schematically illustrated in Scheme 1. Figure 1a–c presents the typical transmission electron microscopy (TEM) images of $NaYbF_4$:Tm (Figure 1a), $NaYbF_4$:Tm@SiO_2 (Figure 1b, NS), and $NaYbF_4$:Tm@SiO_2@$NaYF_4$ (Figure 1c, NSY). The powder X-ray diffraction (XRD) patterns (Figure 1g) and the size distribution diagrams of $NaYbF_4$:Tm@$NaYF_4$ (Figure 1h) reveal that the nanocrystals adopt a hexagonal crystalline structure without any extra phase and exhibit a nearly monodispersive nature. High-angle annular dark-field scanning transmission electron microscopy (HAADF-STEM) (Figure 1j) images showed significant differences; the distribution size of Y element is larger than that of Yb, indicating that the Y element is distributed in the outer layer of the nanocomposite structure, which confirms that the NY upconverting nanoparticles have the core–shell structure. To clarify the authenticity and the mechanism of the interesting results, a series of verification experiments were designed and conducted. We gradually shortened the reaction time of the final step, and the resulting intermediate granular size fully verified our hypothesis that the core–shell particle size should follow a declining trend from more than ~100 to ~20 nm. As the reaction time increases, the size of the generated nanoparticles gradually decreases. Figure 1d–f shows the TEM images of the core–shell $NaYbF_4$:Tm@$NaYF_4$ nanostructure when the reaction times are 55, 75, and 90 min, respectively. Considering that the precursor is the same $NaYbF_4$ nanoparticles in these two synthesis processes, the only difference is the reaction condition including the chemical reagents. Therefore, a reasonable mechanism deduced on the basis of the distinct phenomena could be that the reduction of particle size most likely depends on the solvents or the monomers in the reaction vessels. As a generally accepted crystalline formation mechanism, particle size growth undergoes a usual process, *i.e.*, the larger particle grows at the cost of the smaller one, which is a well-known OR process. However, following an inverse OR process, which is also designated as DR process, the unusual size reduction process during synthesis at the expense of larger grains due to the etching effect of monomers or solvents for instance (such as –SH groups), smaller nanoparticles with uniform dispersion are eventually formed.[34] The crystal structure, grain size, and morphology of lanthanide-doped β-$NaYbF_4$ are highly dependent on its inherent structure and many external factors, such as the reaction time, temperature, pH value of the initial solution, organic additives, purity of dopants, *etc.*[37] Logically, in our synthesis conditions, the partially desorbed ligands coordinated with Yb ions and the temperature work together and decompose the as-prepared nanocrystals into smaller nanostructures. Also, as the reaction goes on, the outer core layer

Scheme 1. Schematic Diagram of the Synthesis Processes of NS (Microemulsion) and NY (DR-Mediated Pyrolysis)[a]

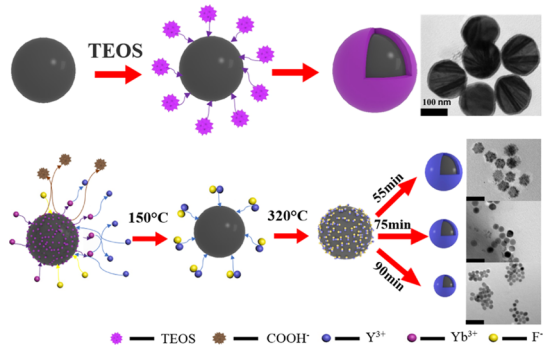

[a]NS and NY denote $NaYbF_4$:Tm@SiO_2 and $NaYbF_4$:Tm@$NaYF_4$ core–shell nanostructures, respectively. The scale bars in TEM images are 100 nm.

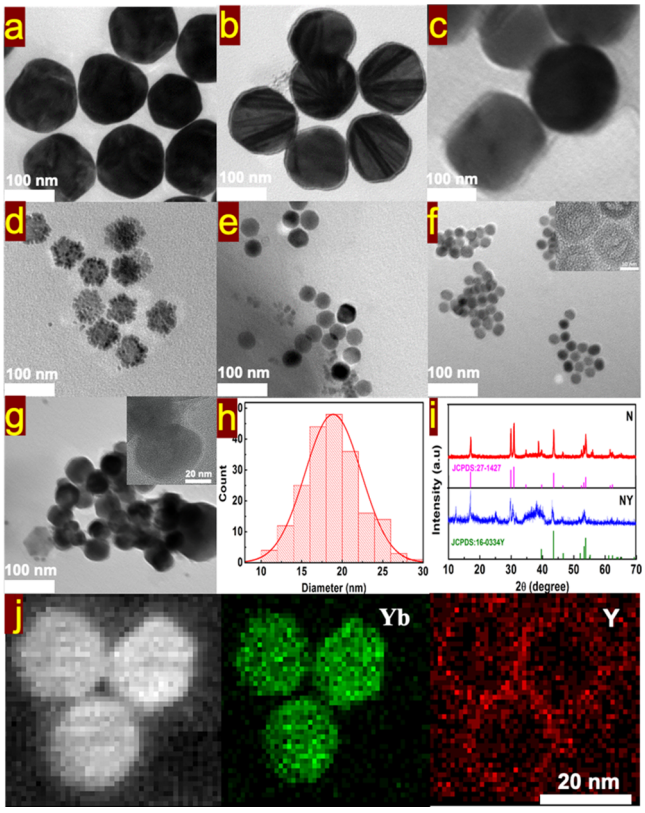

Figure 1. (a) TEM images of N nanoparticles. (b) TEM image of NS. (c) TEM image of NSY. TEM images of NY when the reaction times are (d) 55 min, (e) 75 min, and (f) 90 min. (g) TEM image of NYS. (h) Size distribution of NY from (f). (i) XRD patterns of N and NY. (j) HAADF-STEM image of NY and EDX element mapping images of Yb and Y, respectively. (N denotes $NaYbF_4$ nanoparticles, and NSY denotes the $NaYbF_4$:Tm@SiO_2@$NaYF_4$ nanostructure).

https://dx.doi.org/10.1021/acsanm.0c02057
ACS Appl. Nano Mater. 2020, 3, 10049–10056

partially dissolves during the heating step of the reaction, just analogous to the etching effect in the preparation of gold nanoparticles in the presence of organic solvents.[22]

Fourier transform infrared (FT-IR) spectra in Figure 2a show that on the surface of the $NaYF_4$ nanoshell there are

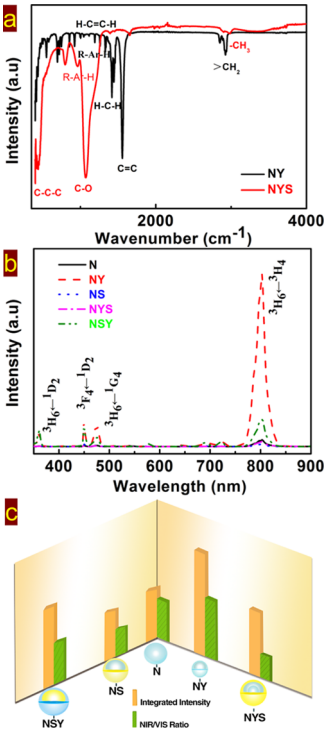

Figure 2. (a) Fourier infrared spectra of NY and NYS. (b) UCL spectra of uncoated N nanocrystals and coated samples with different nanoshells excited by a 980 nm laser. (c) Comparison of UCL intensities of different core−shell structures and the NIR/VIS ratios of N and coated samples pumped by the 980 nm laser. (NYS denotes $NaYbF_4$:Tm @$NaYF_4$@SiO_2 nanocrystals).

indeed some groups of oleic acid and 1-octadenece. The peak at 1450 cm^{-1} originates from H−C−H bond vibration, and the peaks at 2926 and 2853 cm^{-1} originate from saturated $>CH_2$ hydrogen shock, which are consistent with the absorption peak of the standard oleic acid infrared spectrum for a H−C−H single bond vibration at 1450 cm^{-1} alongside $>CH_2$ hydrogen bond vibration at 2866 cm^{-1}. The peak at 1590 cm^{-1} is indexed to C═C double bond vibration; this is consistent with the absorption peak of the C═C double bond vibration at 1497 cm^{-1} in the standard 18 dilute infrared spectra. However, they almost got vanished after an additional coating on the silica shell. This supporting result reveals that in the current study, these groups are playing a crucial role in particle shrinking, following the DR process. The formation of hexagonal columnar β-$NaYF_4$ crystals is reported, involving a hydrothermal transformation process from the metastable mesophase of α-$NaYF_4$ to the thermodynamically stable nucleus of β-$NaYF_4$ and then further growth into stable and larger β-$NaYF_4$ crystals under hydrothermal conditions.[30] Since the K_{SP} of YbF_3 (PK_{SP} (YbF_3) = 16.3) is higher than that of YF_3 (PK_{SP} (YF_3) = 17.3),[38] it is easier for F^- to precipitate Y^{3+} to form YF_3 crystals, rather than Yb^{3+} to form YbF_3. In our synthesis conditions for ternary upconverting nanocrystals with core−shell structures in the oil phase, $NaYbF_4$ and $NaYF_4$ crystal structures form in the solution through the reaction of Y^{3+}, Na^+, and F^- ions. The number of $NaYF_4$ crystals that emerged through the dominant precipitation reaction is far greater than that of $NaYbF_4$ crystals, which will adhere to the surface of $NaYbF_4$, constructing the nanoshell outside the luminescent core. Part of Yb^{3+} on the surface of $NaYbF_4$ is subjected to ionization; under the reaction conditions of an oil phase, $NaYbF_4$ crystal surface free energy changes, and at the same time, Y^{3+} in the solvent continuously combines with F^-, generating more stable YF_3 and thereafter the $NaYF_4$ nanoshells. At the end of the synthesis reaction, a dynamic ionization equilibrium is achieved. As the reaction time increases, the formation rate of $NaYF_4$ is much faster than that of $NaYbF_4$. The coating on the surface of $NaYbF_4$ crystals leads to the smaller size of the product and in turn a decrease in the size of the overall core−shell nanocrystal of $NaYbF_4$:Tm @$NaYF_4$, as shown in Scheme 1.

Upconversion Luminescence Regulation. Figure 2b shows the UCL spectra of $NaYbF_4$:Tm, $NaYbF_4$:Tm@SiO_2, $NaYbF_4$:Tm@SiO_2@$NaYF_4$, $NaYbF_4$:Tm@$NaYF_4$, and $NaYbF_4$:Tm@$NaYF_4$@SiO_2 nanoparticles, featuring the UCL bands of Tm^{3+} at ∼360, 450, 475, and 805 nm, which correspond to the f−f inner-configurational transition of $^1D_2 \rightarrow {}^3H_6$, $^1D_2 \rightarrow {}^3F_4$, $^1G_4 \rightarrow {}^3H_6$, and $^3H_4 \rightarrow {}^3H_6$, respectively. The integrated UCL intensity of $NaYbF_4$:Tm nanoparticles is significantly enhanced by cladding the $NaYF_4$ shell; for instance, the blue band at about 450 nm has been 4.8-fold intensified. However, the upconversion luminescence intensity of the core−shell−shell nanoparticles coated with SiO_2 on the outermost layer was dramatically reduced.

The reason for the enhancement lies in that $NaYF_4$ can prevent the energy transfer in the Yb sublattice from being captured by the surface quencher, thus promoting the excitation efficiency of activators, which plays a protective role in the energy transfer of the excitation energy to Tm^{3+} and improves the upconversion emission.[28,29] As a result, the integrated intensity of NY as shown in Figure 2c is more prominent than that of the pure $NaYbF_4$ core. On the other hand, when the nanocore is coated with a layer of $NaYF_4$, Yb^{3+} ions and the surface quenching agent can be separated well, which largely inhibits quenching.[39,40] However, the quenching of UCL after silica coating results from that the SiO_2 shell promotes the scattering of the excitation light, thus diminishing the excitation efficiency of the pumping light.[40] Strategies for adjusting the UCL color output typically include manipulating dopant/host complexes and dopant concentrations in nanoshell structures.[28] The growth of inert shells on the surface of optically active nanocrystalline nuclei is a common method to reduce the surface quenching process, which can significantly improve the quantum yield.[41] To further verify the manipulation rule by means of coating different types of nanoshells on the UCL properties, $NaYbF_4$:Tm@$NaYF_4$@SiO_2 and $NaYbF_4$:Tm@SiO_2@$NaYF_4$ core−shell−shell nanostructures are successfully prepared and investigated spectroscopically. Compared to the original core−shell nanoparticles, the UCL intensity from Tm ions is quenched remarkably after SiO_2 coating but dramatically enhanced after $NaYF_4$ shell modification. This interesting switchlike effect stemming from the alternant nanoshell coating on the UCL intensity variation trend is depicted in Figure 2c. In short, the inert shell $NaYF_4$ demonstrates a benefit to the fluorescence intensity, whereas the silica shell coating functions the opposite.

https://dx.doi.org/10.1021/acsanm.0c02057
ACS Appl. Nano Mater. 2020, 3, 10049−10056

Figure 2c also shows the NIR/VIS ratio of single and binary nanoshell-coated samples. The variation trend of the NIR/VIS branch ratio from the samples with different compositions of the nanoshell is observed similar to that of the integrated intensity, *i.e.*, when coated with SiO_2 on the surface of the nanoparticles, the NIR/VIS ratio declines significantly, whereas in the case of the $NaYF_4$ nanoshell, the NIR/VIS ratio arises as a consequence. It is worth noting that this manipulation by means of nanoshell engineering is applicable not only to the luminescent core but also to the core−shell counterpart compared to the NIR/VIS ratio of their precursor. The detailed discussion on the mechanism of branch ratio variation with different coating strategies will be demonstrated later.

To verify the UCL mechanism, pumping power dependence of the integrated Tm^{3+} UCL emission intensity (I_{uc}) is plotted in Figure 3a. The UCL intensity, which is a typical nonlinear

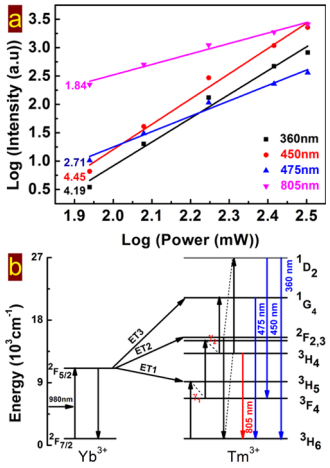

Figure 3. (a) Log−log plots of UCL intensity as a function of the excitation power for $NaYbF_4$:Tm nanocrystals. (b) Schematic energy levels of Yb and Tm ions alongside the possible upconversion transition processes under the excitation of the 980 nm laser.

effect, is generally considered as an *n*-power function of the excitation power density (P). This can be simply described as the following formula: $I_{uc} \propto P^n$, where n is the number of absorbed photons for each radiative transition and its values can be derived from the slope of the linearly fitted line plotted between $\ln(I_{uc})$ and $\ln(P)$. Because of the multiple excitation mechanisms, state decay processes, and energy transfer pathways, the number of photons required each time is not an ideal integer.[42] Therefore, the slope obtained from the fitting is 4.19, 4.45, 2.71, and 1.84, corresponding to the emission at ∼360, 450, 475, and 805 nm, respectively, which implies that these UC processes follow 4-, 4-, 3-, and 2-photon processes and are in agreement with the early results in the literature.[17]

Yb^{3+} generally acts as a sensitizer for upconverting activators due to its larger absorption cross section. The $^2F_{7/2} \rightarrow {}^2F_{5/2}$ transition has good resonance with certain energy levels of upconversion lanthanide ions, which can significantly improve the upconversion efficiency.[43] First, Yb^{3+} ions absorb a 980 nm photon and then the excitation energy is transferred by dipole−dipole to the adjacent Tm^{3+} in the lattice, making the $^3H_5$ energy level populated *via* the energy transfer (ET1) process. Figure 3b depicts the energy levels of the Yb and Tm ions as well as the illustration of possible UCL process between the sensitizer and activator. Thereafter, the excited electrons on the $^3H_5$ energy level relax onto $^3F_4$ nonradiatively (γ_1), followed by absorbing another NIR photon energy and populating the $^2F_{2,3}$ energy levels through the energy transfer process (ET2). The electrons with higher energy on $^2F_{2,3}$ undergo a nonradiative relaxation (γ_2) to the $^3H_4$ state and subsequently transition to the ground state $^3H_6$, giving 805 nm emission ($^3H_4 \rightarrow {}^3H_6$). On the other hand, part of these excited electrons could be pumped to the $^1G_4$ level *via* the energy transfer process (ET3). The radiative transition from the $^1G_4$ level to the ground state $^3H_6$ generates 475 nm emission. However, the emissions at 450 and 360 nm could not be obtained from the excited-state absorption process because of the energy difference between $^1D_2$ and $^1G_4$ levels. The $^1D_2$ level is populated by the cross-relaxation process $^2F_2/{}^2F_3 + {}^3H_4 \rightarrow {}^3H_6 + {}^1D_2$, and finally, the transition from the $^1D_2$ level to the $^3F_4$ and $^3H_6$ levels produces the emission of 450 and 360 nm, respectively.

With the silica coating outside the luminescent core, both the overall UCL intensity and NIR/VIS decrease. The change in the NIR/VIS ratio is most likely because the coating affects the energy transfer process between the excitation source and the activators; the surface quenching center is passivated by silicon dioxide. It can be seen from Figure 2a that after silica epitaxy the absorption of C═C and $>CH_2$ bonds on the crystal surface has been remarkably restrained; this probably means that these groups are the main quenching centers for visible emissions. Meanwhile, C−O bond absorption becomes intensified, which possibly implies that it is the quencher for NIR emission. Thus, on the basis of these deductions, one can reasonably understand that the UCL intensity and NIR/VIS ratio decrease synchronously, which is ascribed to the relatively dramatic quenching of NIR to that of VIS emission.

To further clarify the impact mechanism of nanoshells on luminescence properties, the transient investigation of Tm^{3+} excited states has been carried out before and after coating the $NaYF_4$ nanoshell. Figure 4 shows the attenuation curve of

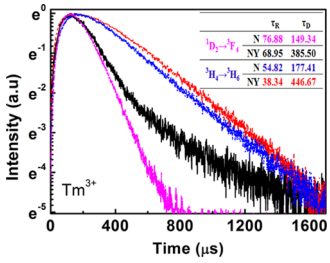

Figure 4. Luminescence decay curves of N and NY excited by the 980 nm laser. Inset: the derived UCL rise and decay times.

Tm^{3+} $^1D_2 \rightarrow {}^3F_4$ and $^3H_4 \rightarrow {}^3H_6$ transitions. Each curve shows a typical rise and decay process, demonstrating a typical UCL energy transfer process. A simplified model can be proposed presenting the time dependence of the UCL emission intensity ($I(t)$) after a short pulse excitation

$$I(t) = Ae^{-t/\tau_D} - Ae^{-t/\tau_R} \quad (1)$$

where A is the emission intensity factor and τ_D and τ_R represent the transient decay and rising times of nonlinear UCL transition process, respectively. The decay time (τ) is calculated by

https://dx.doi.org/10.1021/acsanm.0c02057
ACS Appl. Nano Mater. 2020, 3, 10049−10056

$$\tau = \frac{1}{I_0}\int_0^\infty I(t)\mathrm{d}t \quad (2)$$

where $I(t)$ denotes the luminescence intensity dependent on time t and I_0 represents the maximum intensity, thereby achieving the corresponding UCL lifetime, as shown in the inset of Figure 4 (in the unit of microseconds).

The results showed that the UCL lifetime of the nanoparticles coated with a layer of $NaYF_4$ was prolonged. The lifetime of an excited state (τ) is determined by the radiative transition rate (W_R), the nonradiative transition rate (W_{NR}), and the energy transfer rate (W_{ET}), which can be expressed as

$$\tau \propto 1/(W_R + W_{NR} + W_{ET}) \quad (3)$$

The $NaYF_4$ shell is adopted to realize passivation, and it effectively prevents the excitation from being captured by the surface quenching centers.[28] The shell can minimize surface defects and protect the optically excited Tm^{3+} ions in the core from deactivation with high-energy vibration such as surface ligands or solvent molecules, which can interact with the excited state of Yb^{3+} through dipole−dipole interactions.[44] Therefore, the lifetime increased as a consequence of the reduced nonradiative transition probability. This additionally confirms our previous arguments on the increased overall UCL intensity. Also, after coating a layer of $NaYF_4$, the population of $^1D_2$ and $^3H_4$ states increases but that of $^3H_4$ exhibits more prominence than that of $^1D_2$; thus, the cross-relaxation process ($^2F_{2,3}$−$^3H_6$, $^3H_4$−$^1D_2$) is impeded, leading to a longer fluorescence lifetime and an enhanced NIR/VIS ratio, as shown in Figure 2c.

CONCLUSIONS

An unprecedented DR-mediated growth process has been observed in the preparation of ternary fluoride upconverting core−shell nanostructures. The uniform particle size decreases as the reaction time is prolonged. This DR process could be reasonably considered to be related to the K_{sp} values of YbF_3 and YF_3 during the nucleation process. Through coating different nanoshells, *i.e.*, silica and $NaYF_4$, with alternate compositions, the UCL intensity as well as the NIR/VIS ratio has been facilely controlled. After silica coating, the overall luminous intensity and the ratio are reduced; however, after $NaYF_4$ coating, the overall luminous intensity and the ratio are enhanced. Our findings provide a promising method for the preparation of monodispersed nanoscale core−shell particles from the larger ones; meanwhile, the UCL properties could be simultaneously regulated by means of core−shell engineering.

ASSOCIATED CONTENT

Supporting Information

The Supporting Information is available free of charge at https://pubs.acs.org/doi/10.1021/acsanm.0c02057.

HAADF-STEM of NSY; X-ray photoelectron spectroscopy (XPS) of NY, NSY, and NYS; energy-dispersive X-ray spectroscopy of NY; and the quantum yields of NY and N (PDF)

AUTHOR INFORMATION

Corresponding Author

Li Chen − *School of Chemistry and life Sciences, Advanced Institute of Materials Science and School of Materials Science and Engineering, Changchun University of Technology, Changchun, Jilin 130012, China;* orcid.org/0000-0003-2504-5793; Email: chenli@ccut.edu.cn

Authors

Chunyu Qi − *School of Chemistry and life Sciences, Advanced Institute of Materials Science, Changchun University of Technology, Changchun, Jilin 130012, China*

Yuan Gao − *School of Chemistry and life Sciences, Advanced Institute of Materials Science, Changchun University of Technology, Changchun, Jilin 130012, China*

Yue Wang − *School of Chemistry and life Sciences, Advanced Institute of Materials Science, Changchun University of Technology, Changchun, Jilin 130012, China*

Jing Li − *School of Materials Science and Engineering, Changchun University of Technology, Changchun, Jilin 130012, China*

Ligong Zhang − *State Key Laboratory of Luminescence and Applications, Changchun Institute of Optics, Fine Mechanics and Physics, Chinese Academy of Sciences, Changchun 130033, China*

Yongshi Luo − *State Key Laboratory of Luminescence and Applications, Changchun Institute of Optics, Fine Mechanics and Physics, Chinese Academy of Sciences, Changchun 130033, China*

Xiaojun Wang − *Department of Physics, Georgia Southern University, Statesboro, Georgia 30460, United States*

Complete contact information is available at: https://pubs.acs.org/10.1021/acsanm.0c02057

Author Contributions

C.Q. carried out most of the experiments and prepared the draft of the manuscript with input from Y.G., Y.W., and J.L. L.Z. and Y.L. assisted in the transient optical measurements. X.W. edited the manuscript and discussed the results. L.C. initiated the research and conceived the experiments. All authors have given approval to the final version of the manuscript.

Notes

The authors declare no competing financial interest.

ACKNOWLEDGMENTS

The authors greatly acknowledge the financial support from the National Natural Science Foundation of China (Nos. 11474035 and 11504029), the Natural Science Foundation supported by the Science & Technology Department of Jilin Province (Grant No. 20200201247JC), and the Jilin Province Education Department (Grant No. JKH20200646KJ).

REFERENCES

(1) Auzel, F. Upconversion and anti-stokes processes with f and d ions in solids. *Chem. Rev.* **2004**, *104*, 139−174.

(2) Zhang, J. H.; Hao, Z. D.; Li, J.; Zhang, X.; Luo, Y. S.; Pan, G. H. Observation of efficient population of the red-emitting state from the green state by non-multiphonon relaxation in the Er^{3+}−Yb^{3+} system. *Light: Sci. Appl.* **2015**, *4*, No. e239.

(3) Wang, J.; Zhang, H.; Ni, D. L.; Fan, W. P.; Qu, J. X.; Liu, Y. Y.; Jin, Y. Y.; Cui, Z. W.; Xu, T. Y.; Wu, Y.; Bu, W. B.; Yao, Z. W. High-Performance Up-conversion Nanoprobes for Multimodal MR Imaging of Acute Is-chemic Stroke. *Small* **2016**, *12*, 3591−3600.

(4) Xu, M.; Chen, D. Q.; Huang, P.; Wan, Z. Y.; Zhou, Y.; Ji, Z. G. A Dual-Functional Up-conversion Core@Shell Nanostructure for White Light-Emission and Temperature Sensing. *J. Mater. Chem. C* **2016**, *4*, 6516−6524.

(5) Zhu, X. J.; Feng, W.; Chang, J.; Tan, Y. W.; Li, J. C.; Chen, M.; Sun, Y.; Li, F. Y. Temperature-Feedback Up-conversion Nanocomposite for Accurate Photothermal Therapy at Facile Temperature. *Nat. Commun.* **2016**, *7*, No. 10437.
(6) Hu, Y. Q.; Shao, Q. Y.; Deng, X. Y.; Han, S. Y.; Song, D. D.; Jiang, J. Q. Core/Shell Up-conversion Nanocrystal Hybrids with Temperature-Dependent Emission Color Changes for Multilevel Anticounterfeiting Applications. *Adv. Mater. Technol.* **2018**, *4*, No. 1800498. (1-5).
(7) Tian, G.; Gu, Z. J.; Zhou, L. J.; Yin, W. Y.; Liu, X. X.; Yan, L.; Jin, S.; Ren, W. L.; Xing, G. M.; Li, S. J.; Zhao, Y. L. Mn^{2+} Dopant-Controlled Synthesis of $NaYF_4$:Yb/Er Up-conversion Nanoparticles for in Vivo Imaging and Drug Delivery. *Adv. Mater.* **2012**, *24*, 1226−1231.
(8) Wang, F.; Han, Y.; Lim, C. S.; Lu, Y. H.; Wang, J.; Xu, J.; Chen, H. Y.; Zhang, C.; Hong, M. H.; Liu, X. G. Simultaneous Phase and Size Control of Up-conversion Nanocrystals through Lanthanide Doping. *Nature* **2010**, *463*, 1061−1065.
(9) Tang, J.; Chen, L.; Li, J.; Wang, Z.; Zhang, J. H.; Zhang, L. G.; Luo, Y. S.; Wang, X. J. Selectively enhanced red upconversion luminescence and phase/size manipulation via Fe^{3+} doping in $NaYF_4$:Yb,Er nanocrystals. *Nanoscale* **2015**, *7*, 14752−14759.
(10) Hu, Y. Q.; Shao, Q. Y.; Dong, Y.; Jiang, J. Q. Energy Loss Mechanism of Up-conversion Core/Shell Nanocrystals. *J. Phys. Chem. C* **2019**, *123*, 22674−22679.
(11) Chen, B.; Wang, F. Recent advances in the synthesis and application of Yb-based fluoride upconversion nanoparticles. *Inorg. Chem. Front.* **2020**, *7*, 1067−1081.
(12) Dahlberg, K. A.; Schwank, J. W. Synthesis of Ni@SiO_2 Nanotube Particles in a Water-in-Oil Microemulsion Template. *Chem. Mater.* **2012**, *24*, 2635−2644.
(13) Wang, X. J.; Zhu, Q.; Li, J. G. Eu^{3+} Doped La_2O_3 Nano Phosphors: Hydrothermal Synthesis and Optical Properties. *J. Rare Earths* **2013**, *06*, 641−647.
(14) Doerner, H. A.; Hoskins, W. M. Co-Precipitation of radium and barium sulfates. *J. Am. Chem. Soc.* **1925**, *47*, 662−675.
(15) Atkins, T. M.; Thibert, A.; Larsen, D. S.; Dey, S.; Browning, N. D.; Kauzlarich, S. M. Femtosecond Ligand/Core Dynamics of Microwave-Assisted Synthesized Silicon Quantum Dots in Aqueous Solution. *J. Am. Chem. Soc.* **2011**, *133*, 20664−20667.
(16) Ansari, A. A.; Yadav, R.; Rai, S. B. Enhanced luminescence efficiency of aqueous dispersible $NaYF_4$:Yb/Er nanoparticles and the effect of surface coating. *RSC Adv.* **2016**, *6*, 22074−22082.
(17) Shi, R. K.; Ling, X. C.; Li, X. N.; Zhang, L.; Lu, M.; Xie, X. J.; Huang, L.; Huang, W. Tuning hexagonal $NaYbF_4$ nanocrystals down to sub-10 nm for enhanced photon upconversion. *Nanoscale* **2017**, *9*, 13739−13746.
(18) Johnson, N. J.; Korinek, A.; Dong, C. H.; Vanveggel, F. C. J. M. Self-Focusing by Ostwald Ripening: A Strategy for Layer-by-Layer Epitaxial Growth on Upconverting Nanocrystals. *J. Am. Chem. Soc.* **2012**, *134*, 11068−11071.
(19) Lee, D. K.; Park, S. I.; Lee, J.; Hwang, N. M. A theoretical model for digestive ripening. *Acta Mater.* **2007**, *55*, 5281−5288.
(20) Prasad, B. L. V.; Stoeva, S. I.; Scorensen, C. M.; Klabunde, K. J. Digestive Ripening of Thiolated Gold Nanoparticles: The Effect of Alkyl Chain Length. *Langmuir* **2002**, *18*, 7515−7520.
(21) Han, S. Y.; Deng, R. R.; Xie, X. J.; Liu, X. J. Enhancing luminescence in Lanthanide-Doped up-conversion Nanoparticles. *Angew. Chem., Int. Ed.* **2014**, *53*, 11702−11715.
(22) Cong, T.; Ding, Y. D.; Hong, X.; Liu, Y. C. Host lattice manipulation-induced up-conversion luminescence modulation through diatomic metal ions intervening. *Nanomedicine* **2018**, *14*, 1745.
(23) Raymo, F. M.; Tomasulo, M. Electron and energy transfer modulation with photochromic switches. *Chem. Soc. Rev.* **2005**, *34*, 327−336.
(24) Swabeck, J. K.; Fischer, S.; Bronstein, N. D.; Paul Alivisatos, A. Broad-band Sensitization of Lanthanide Emission with Indium Phosphide Quantum Dots for Visible to Near-Infrared Downshifting. *J. Am. Chem. Soc.* **2018**, *140*, 9120−9126.
(25) Zhang, H.; Li, Y. J.; Ivanov, I. A.; Qu, Y. Q.; Huang, Y.; Duan, X. Plasmonic modulation of the upconversion fluorescence in $NaYF_4$:Yb/Tm hexaplate nanocrystals using gold nanoparticles or nano shells. *Angew. Chem., Int. Ed.* **2010**, *49*, 2865−2868.
(26) Kuang, Y.; Xu, J. T.; Wang, C.; Li, T. Y.; Gai, S. L.; He, F.; Yang, P. P.; Lin, J. Fine-Tuning Ho-Based Red-Upconversion Luminescence by Altering $NaHoF_4$ Core Size and $NaYbF_4$ Shell Thickness. *Chem. Mater.* **2019**, *31*, 7898−7909.
(27) Lee, H. H.; Racicot, R. J.; Lee, S. H. Surface passivation of GaAs. *Appl. Phys. Lett.* **1989**, *54*, 724−726.
(28) Quintanilla, M.; Fu, Q. R.; Ma, D. L.; Vetrone, F. Light Management in Upconverting Nanoparticles: Ultrasmall Core/Shell Architectures to Tune the Emission Color. *ACS Photonics* **2014**, *1*, 662−669.
(29) Su, Q. Q.; Han, S. Y.; Xie, X. J.; Zhu, H. M.; Chen, H. Y.; Chen, C. K.; Liu, R. S.; Chen, X. Y.; Wang, F.; Liu, X. G. The Effect of Surface Coating on Energy Migration-Mediated Up-conversion. *J. Am. Chem. Soc.* **2012**, *134*, 20849−20857.
(30) Zhang, H. X.; Fan, Y.; Pei, P.; Sun, C. X.; Liu, L. F.; Zhang, F. Tm^{3+}-Sensitized NIR-II Fluorescent Nanocrystals for In Vivo Information Storage and Decoding. *Angew. Chem., Int. Ed.* **2019**, *58*, 10153−10157.
(31) Liu, L.; Wang, S. W.; Zhao, B. Z.; Pei, P.; Fan, Y.; Li, X. M.; Zhang, F. Er^{3+} Sensitized 1530 nm to 1180 nm Second Near-Infrared Window Upconversion Nanocrystals for In Vivo Biosensing. *Angew. Chem., Int. Ed.* **2018**, *57*, 7518−7522.
(32) Liu, L.; Li, X. M.; Fan, Y.; Wang, C. Y.; El-Toni, A. M.; Alhoshan, M. S.; Zhao, D. Y.; Zhang, F. Elemental Migration in Core/Shell Structured Lanthanide Doped Nanoparticles. *Chem. Mater.* **2019**, *31*, 5608−5615.
(33) Chen, B.; Kong, W.; Wang, N.; Zhu, Z. Y.; Wang, F. Oleylamine-Mediated Synthesis of Small $NaYbF_4$ Nanoparticles with Tunable Size. *Chem. Mater.* **2019**, *31*, 4779−4786.
(34) Irzhak, T. F.; Irzhak, V. I. On the Digestive Ripening Mechanism. *Dokl. Phys. Chem.* **2019**, *486*, 77−79.
(35) Tang, J.; Chen, L.; Xie, W. Y.; Liu, W. J.; Huang, Y. X.; Li, J.; Zhang, L. G.; Luo, Y. S. Upconversion Luminescence of $NaYF_4$:Yb,Er Nanocrystals Co-doped with $3d^5$ Metal Ions. *Chin. J. Lumin.* **2016**, *37*, 1056−1065.
(36) Shi, F.; Zhai, X. S.; Zheng, K.; Z, D.; Qin, W. P. Synthesis of monodisperse $NaYF_4$:Yb,Tm@SiO_2 nanoparticles with intense ultraviolet upconversion luminescence. *J. Nanosci. Nanotechnol.* **2011**, *11*, 9912−9915.
(37) Zhou, T.; Luo, R.; Li, Y. M.; Li, T.; Zhao, Y.; Liu, M. J.; Lai, X.; Bi, J.; Gao, D. J. Yb^{3+}, Tm^{3+} Co-doped β-NaY1-xGdxF4 ($0 \leq x \leq 1.00$) microcrystals: Hydrothermal synthesis, evolution of microstructures and up-conversion luminescence properties. *J. Lumin.* **2019**, *211*, 363−374.
(38) Burgess, J.; Kijowski, J. Lanthanide, yttrium and scandium trihalides, Preparation of anhydrous materials and solution thermochemistry. *Adv. Inorg. Chem. Radiochem.* **1981**, *24*, 57−114.
(39) Huang, B. R.; Bergstrand, J.; Duan, S.; Zhan, Q. Q.; Widengren, J.; Agren, H.; Liu, H. C. Overtone Vibrational Transition Induced Lanthanide Excited-State Quenching in Yb^{3+}/Er^{3+}-Doped Up-conversion Nanocrystals. *ACS Nano* **2018**, *12*, 10572−10575.
(40) Hu, Y. Q.; Shao, Q. Y.; Dong, Y.; Jiang, J. Q. Energy Loss Mechanism of Upconversion Core/Shell Nanocrystals. *J. Phys. Chem. C* **2019**, *123*, 22674−22679.
(41) Li, Z. Q.; Wang, L. M.; Wang, Z. Y.; Liu, X. H.; Xiong, Y. J. Modification of $NaYF_4$:Yb,Er@SiO_2 Nanoparticles with Gold Nanocrystals for Tunable Green-to-Red Up-conversion Emissions. *J. Phys. Chem. C* **2011**, *115*, 3291−3296.
(42) Fischer, S.; Bronstein, N. D.; Swabeck, J. K.; Chan, E. M.; Alivisatos, A. P. Precise tuning of surface quenching for luminescence enhancement in core-shell lanthanide-doped nanocrystals. *Nano Lett.* **2016**, *16*, 7241−7247.

https://dx.doi.org/10.1021/acsanm.0c02057
ACS Appl. Nano Mater. 2020, 3, 10049−10056

(43) Tu, L. P.; Liu, X. M.; Wu, F.; Zhang, H. Excitation energy migration dynamics in up-conversion nanomaterials. *Chem. Soc. Rev.* **2015**, *44*, 1331−1345.
(44) Würth, C.; Fischer, S.; Grauel, B.; Alivisatos, A. P.; Genger, U. R. Quantum yields, surface quenching and passivation efficiency for ultra-small core/shell upconverting nanoparticles. *J. Am. Chem. Soc.* **2018**, *140*, 4922−4928.

https://dx.doi.org/10.1021/acsanm.0c02057
ACS Appl. Nano Mater. 2020, 3, 10049−10056